FIRST STEPS TOWARDS A 3D LOW CYCLE FATIGUE ANALYSIS OF LIQUID ROCKET COMBUSTION CHAMBER WALLS

G. de Boisvilliers
FH Aachen, Aachen, Germany

O.J. Haidn, J.R. Riccius, E.B. Zametaev
German Aerospace Center (DLR), Institute of Space Propulsion, Lampoldshausen, Germany

Abstract

A coupled thermal and structural 3d quasi stationary Finite Element analysis of a typical rocket combustion chamber wall during a full cycle including pre cooling, hot run, post cooling and relaxation is presented. The results of this 3d analysis are compared with the results of 2d plane strain and 2d generalized plane strain analyses. Finally, a post- processing method is applied in order to estimate the life time of the combustion chamber.

Introduction

The extreme thermal loads together with the regenerative cooling of combustion chambers of cryogenic liquid rocket engines introduce enormous temperature gradients in the combustion chamber wall and cause large heat fluxes and induce extremely large thermal stresses. The resulting plastic deformations of the wall material finally limit the combustion chamber life to typically less than 50 operational cycles. Fig 1 shows the scheme of a typical gas generator engine with regenerative cooling.

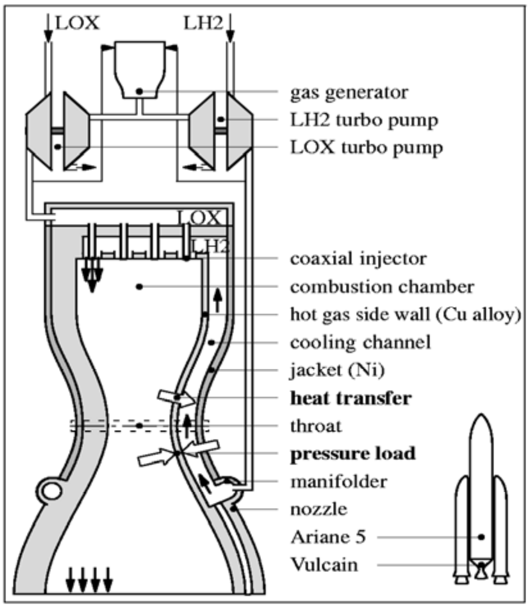

Fig 1. Schematic view of a typical regeneratively cooled combustion chamber

Fig 2 shows a sketch of a typical combustion chamber cross section, emphasizing the characteristic features of a regenerative cooled combustion chamber, such as cooling channel and fin geometry, chamber wall and outer liner materials and liner failure location.

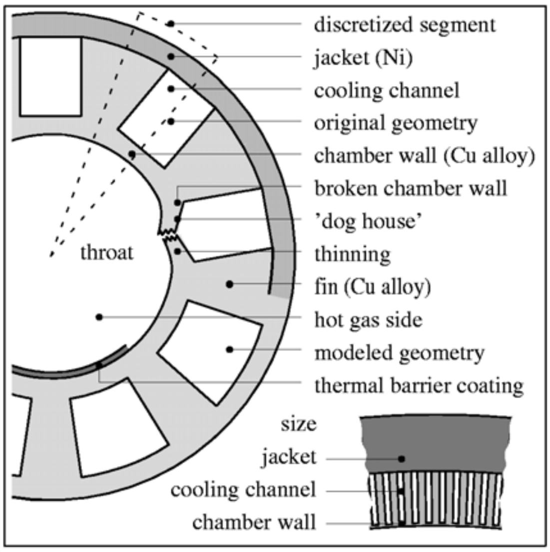

Fig 2. Modeling and characteristic failure

Motivation

The increasing requirements regarding reliability and performance of cryogenic liquid rocket engines in combination with the need to continuously reduce both production and operational cost has led to the idea of reusable space transportation systems (RLV). With 50 or more cycles being a typical life requirement for such a system and nowadays combustion chambers having cycles-to-failure numbers of about 20 or less, the current research and technology activities at DLR Lampoldshausen aim e.g. at a detailed understanding of the failure mechanisms and the development of a verified tool for the prediction of the combustion chamber life [1].

An earlier investigation aiming into the optimization of the cooling channel geometry [2] has shown that the applied material model and life time estimation method have a dramatic influence on the optimization result. This work also demonstrated the importance of the proper choice of elasto-plastic material parameters and the accurate description of the material in an appropriate non-linear material model. With these findings in mind, a wide series of different material tests was performed [3], [4].

In earlier contributions, only 2d Finite Element analyses were presented. In the current paper, 3d results are shown as well and the differences between these analyses are discussed.

General Approach

A full analysis of a given combustion chamber wall is obtained by a successive (one way coupled) analysis of the following sub problems:

- one dimensional stationary thermo-fluid-mechanical analysis of the system hot gas - combustion chamber wall - coolant
- either a 2d or a 3d thermal analysis of the combustion chamber wall during the hot run
- either a 2d or a 3d nonlinear structural analysis of the combustion chamber wall under cyclic thermal and mechanical loading
- post processing life time estimation of the combustion chamber wall

On the hot gas side of the combustion chamber wall, the Bartz equation [5] is applied and film coefficients from experiments are chosen. On the coolant side, a one-dimensional thermo-fluid mechanical approach is used, taking into account empirical models for the heat transfer and fluid mechanical losses. The circumferential variation of the local wall heat flux into the cooling channel is taken into account by using a two dimensional Finite Element model for the simulation of the thermal field within the wall structure. No stratification effects of the cooling channel flow are taken into account in the currently presented work. However, thermal stratification models have been successfully implemented at DLR Lampoldshausen and applied for pure thermo-fluid-mechanical analyses [6]. In the framework of a comparative study, the film coefficients, obtained by the one dimensional thermo-fluid-mechanical analysis, are used to perform either a 2d or a 3d thermal Finite Element Analysis of the combustion chamber wall.

The resulting thermal fields are used as boundary conditions for a 2d plane strain, a 2d generalized plane strain or a 3d analysis of the combustion chamber wall. A standard multilinear elasto-plastic structural analysis method with the von Mises yield function and isotropic hardening is used to analyze the structural behavior of the combustion chamber wall under cyclic thermal and mechanical loading. For an analysis of the low cycle fatigue life of the combustion chamber wall, a simple post processing method is applied, taking into account cyclic and quasi static fatigue as well as the aging of the material. The solution methods for the thermal, structural and life time analyses are discussed in detail in the following sections.

Thermal analysis

In this section, the applied boundary conditions and results of the thermal analysis of the combustion chamber wall are shown. The basic equations and the specification of the material parameters are described in detail e.g. in [7].

Material parameters

The thermal conductivity λ and the heat capacity c are defined temperature dependent. A visualization of these parameter values is given in [7]. A description of the determination of these material parameters is given in [8].

Geometric assignment of boundary conditions

The geometric assignment of the thermal boundary conditions for the analyzed part of the combustion chamber wall is given in Fig 3.

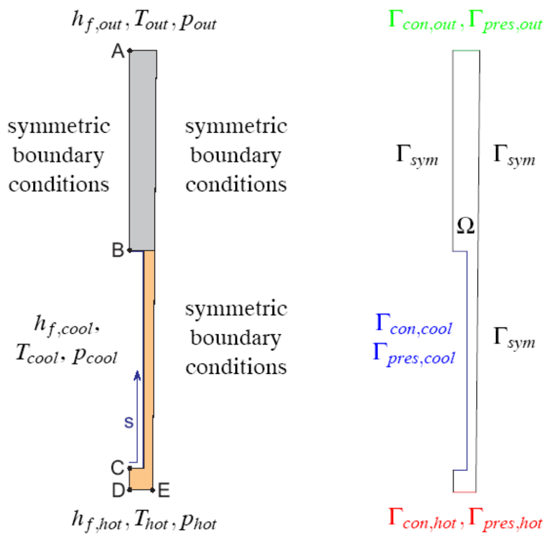

Fig 3. Geometric assignment of the thermal and mechanical boundary conditions for the analyzed part of the combustion chamber wall

These boundary conditions are described in more detail in [7].

Results of the 2d thermal analyses

The results of the 2d thermal analyses of the combustion chamber wall are shown in Fig. 4.

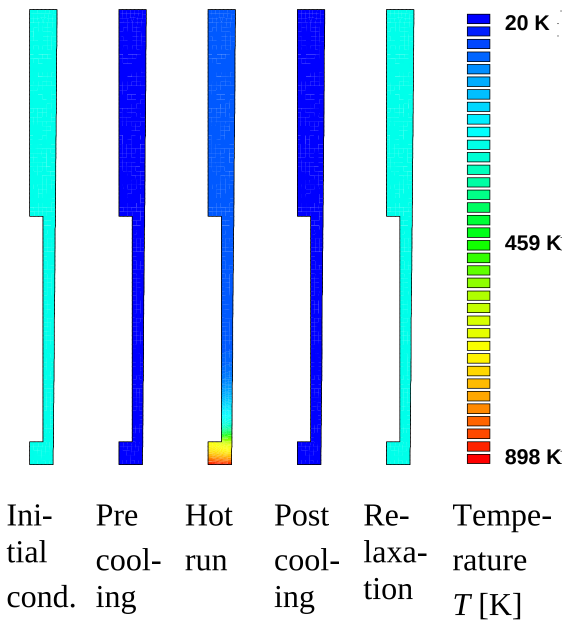

Fig. 4. Distribution of the wall temperature T for the 2d analyses

A linear variation between the different thermal fields is assumed as a thermal boundary condition for the follow-on structural analysis.

Results of the 3d thermal analyses

The thermal field, obtained by the stationary 3d thermal analysis of the combustion chamber wall during the hot run is shown in Fig 5.

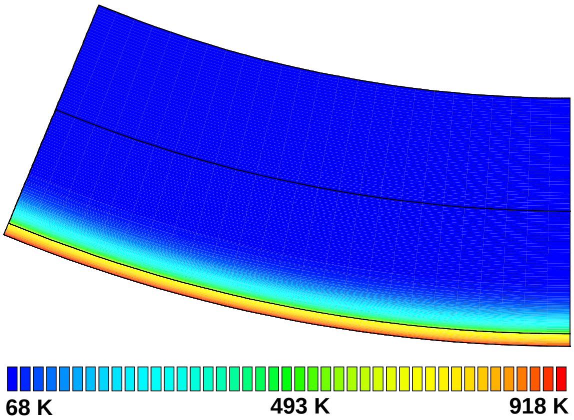

Fig 5. Distribution of the wall temperature *T* for the 3d analysis of the combustion chamber wall during the hot run

Although identical film coefficients and bulk temperatures were used for the 2d and 3d analysis, the maximum temperature for the 3d analysis as shown in Fig 5 is higher than the maximum temperature of the 2d analysis as shown in Fig. 4. This effect is certainly caused by the fact, that for the 3d analysis, the axial length of the cooling part on the outside of the combustion chamber in is smaller than the axial length of the hot gas side. In comparison to the 2d analysis, where the length of the model in axial direction is assumed to be constant, this leads to a loss of cooling power and therefore, to an increased hot gas side wall temperature for the 3d analysis.

Nonlinear structural analysis

Basic Equations

The following model specifications were applied for the Finite Element analyses:

- 2d plane strain, 2d generalized plane strain or fully 3d model
- geometric nonlinearity
- multilinear elasto-plasticity based on the von Mises yield function and isotropic hardening

The basic equations are described in detail e.g. in [7].

Geometric assignment of boundary conditions

The geometric assignment of the boundary conditions is given in Fig 3.

Pressure boundary conditions

The pressure values as given in Table 1 are linearly interpolated between the different stages of the cyclic loading and applied as pressure boundary conditions.

Table 1: Pressure boundary conditions for structural analyses

Stage	Time *t [s]*	coolant pressure *p [MPa]*	hot gas pressure *p [MPa]*
pre cooling	0-2	2	0
hot run	2-902	13.4	10.0
post cooling	902-904	2	0
relaxation	904-1000	0	0

Material parameters

The determination of the structural material parameters is described e.g. in [4].

Results of the structural analyses

A 2d plane strain, 2d generalized plane strain and a 3 d structural Finite Element analyses were performed.

The circumferential total strains in the nozzle cross section are plotted in Fig 6.

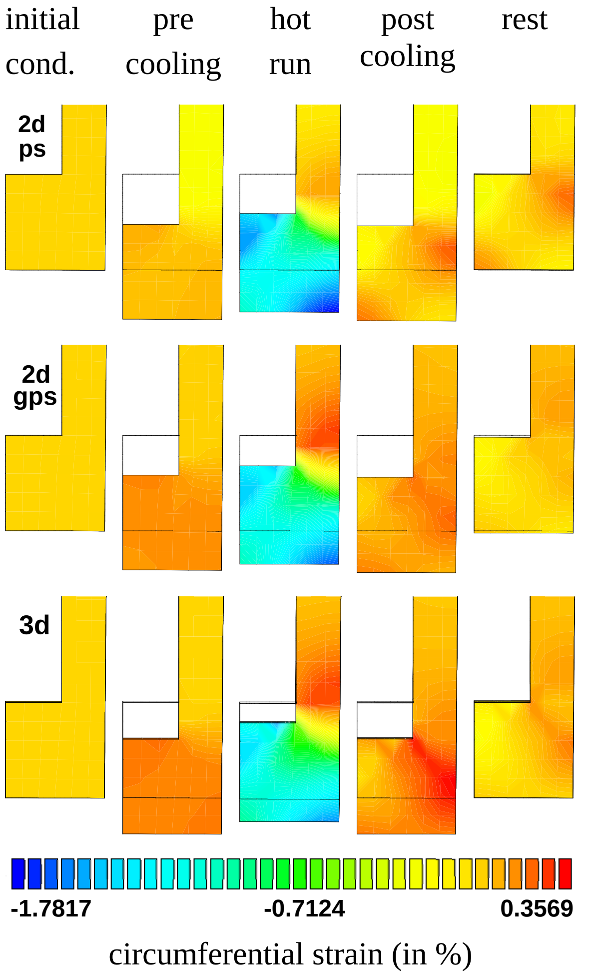

Fig 6. Circumferential total strains in the nozzle cross section for the 2d plane strain (ps) analysis, the 2d generalized plane strain (gps) analysis and the 3d analysis during pre cooling, hot run, post cooling and rest phase

As can be seen in Fig 6, the radius of the combustion chamber is reduced by up to 0.5 mm in the stationary hydrogen **pre- and post-cooling states**. This contraction is due to the temperature reduction of the complete combustion chamber wall by more than 250 degrees. During the stationary **hot run phase** (Fig 6 middle left), very high temperature differences occur in different parts of the combustion chamber wall:

- The nickel layer has a temperature of approximately 68 K, which is significantly less than the initial temperature.
- The hot gas side of the combustion chamber wall is heated up strongly, reaching a maximum temperature of about 900 K.

Therefore, the nickel jacket tends to contract and the copper alloy on the hot gas side of the combustion chamber wall tends to expand. Due to the larger thickness of the nickel jacket in comparison to the hot gas wall and the higher yield strength of nickel in comparison to the yield strength of the copper alloy, the nickel layer imposes its contraction to the copper alloy on the hot gas side. This causes a large plastic compressive straining of the hot gas side wall material.

In the post cooling and rest phase (Fig 6 right), a small fraction of the compressive straining remains in the symmetry points of the fin (point E), while tensile strains are built up in points, situated on the symmetry line of the cooling channels (point D). This can be seen in more detail in Fig 7, where the circumferential stresses are plotted over the circumferential strains in the nozzle cross section.

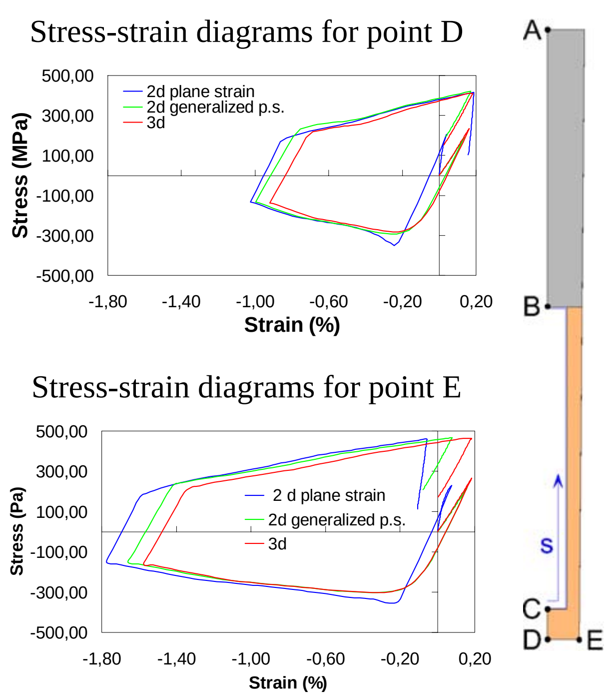

Fig 7. Circumferential stress-strain diagrams, obtained by the 2d plane strain, 2 d generalized plane strain and the 3 d structural analysis

For both considered points D and E, the loading-deformation process starts in the first cycle with zero stresses and zero strains.

During the pre-cooling process, tensile circumferential stresses and strains occur in both considered points. This is due to the higher thermal expansion ratio of the copper alloy (used as the inner wall material) in comparison to the expansion ratio of nickel (used as the jacket material).

At the transition to the hot run phase, compressive stresses are built up at the hot gas side of the combustion chamber wall, causing a high plastic compressive straining of the wall material for both considered points. Due to the temperature dependency of the yield stress, local minima of the stress values occur during the heating up phase. After having reached their minimum, the stress values increase again, because the yield stress is reduced by the increasing wall temperature.

In the post cooling state, tensile stresses reappear. The maximal strain differences per cycle for the selected points D and E and the values of the remaining straining after the full cycle provide the basis for the life time calculation in the following section.

Life time estimation

A post processing approach is chosen for the estimation of the life time of the combustion chamber wall. Three different failure mechanisms are taken into account: cyclic fatigue, quasi static fatigue and thermal aging.

Cyclic fatigue

The life time calculation for the cyclic fatigue part is based on experimental results [9] for the low cycle fatigue behavior of the combustion chamber wall material as shown in Fig 8.

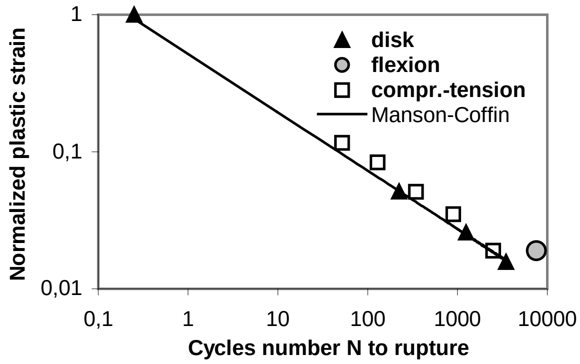

Fig 8. Normalized results of low cycle fatigue experiments for a typical combustion chamber material

As a result of the calculations from the previous section, a cyclic total strain difference can be obtained for any considered position in the structure. From this strain difference and the fitted line from Fig 8, the number of cycles until failure N_c can be obtained easily.

The cyclic fatigue usage factor u_c is calculated as:

$$u_c = \frac{1}{N_c} \tag{1}$$

Usage factors are assumed to add up for each passed cycle and therefore, after N_c identical cycles, a usage factor of $N_c = 1.0$ is obtained, which indicates failure.

Quasi static fatigue

The quasi static usage factor u_{qs} is defined as:

$$u_{qs} = \frac{\max(0,(\varepsilon_{end} - \varepsilon_{begin}))}{\varepsilon_u} \tag{2}$$

with:

ε_{end}	remaining strain after the considered cycle
ε_{begin}	strain at the beginning of the considered cycle
ε_u	ultimate strain of the combustion chamber wall material

After $N_{qs} = \dfrac{1}{u_{qs}}$ identical cycles, the ultimate strain ε_u is obtained, which indicates failure. In the simplest case, the ultimate strain ε_u is assumed to be constant over time. A more sophisticated determination of ε_u dependent on temperature and time is described in the following section.

Thermal degradation of the material

According to [10], the ultimate strain ε_u can be defined dependent on the accumulated run time and the temperature of the considered part of the engine:

$$\varepsilon_u = \varepsilon_u(T,\tau) = B_k \cdot \varepsilon_u(T,0) \cdot \left(\frac{\tau_0}{\tau}\right)^{k_e \cdot m_\sigma(T)} \tag{3}$$

with:

B_K	parameter, taking into account the 3-dimensionality of the deformation
$\varepsilon_u(T,0)$	temperature dependent initial ultimate strain
τ_0	test time for tensile test
τ	accumulated run time of the engine
k_e	exponent weighting factor

The thermal degradation exponent m_σ is specified by equation (4):

$$m_\sigma = 0.001 \cdot e^{\beta \cdot T} \tag{4}$$

with: β : temperature weighting factor

Total fatigue

The total usage factor u_t is defined as the sum of the cyclic and quasi static usage factors:

$$u_t = u_c + u_{qs} \tag{5}$$

Finally, the total number of cycles until failure N_t is calculated as the reciprocal value of the total usage factor u_t :

$$N_t = \frac{1}{u_t} \tag{6}$$

Material parameters

All the material parameters that are needed for the analyses described in the previous sections were completely determined for a copper alloy, which is used as the inner liner material of a recently tested model combustor at DLR Lampoldshausen [6]. As the thermal degradation parameters were not determined yet for this copper alloy, the parameters for a similar copper alloy as given in [10] were chosen for the analyses presented in this section.

Results of the life time estimation

The estimated number of cycles until failure for the 2d plane strain, 2d generalized plane strain and the 3 d analysis are given in Table 2.

Table 2: Estimated number of cycles until failure for points D and E

type of FE analysis	type of LCF estimation		cycles to failure	
			Point	
			D	E
2d plane strain Finite Element analysis	cyclic fatigue only		280	106
	cyclic and quasi static fatigue	with constant ultimate strain	85	106
		with degradation of the ultimate strain	61	106
2d generalized plane strain Finite Element analysis	cyclic fatigue only		305	111
	cyclic and quasi static fatigue	with constant ultimate strain	193	111
		with degradation of the ultimate strain	160	111
3d Finite Element analysis	cyclic fatigue only		348	119
	cyclic and quasi static fatigue	with constant ultimate strain	236	116
		with degradation of the ultimate strain	200	114

The results in Table 2 show an increase of the estimated number of cycles until failure, if a 2d generalized plane strain or a 3d Finite Element analysis is performed instead of a conventional 2d plane strain analysis. Both, the cyclic fatigue part and the quasi static fatigue part contribute to this result.

Reason for the increase of the cyclic fatigue

The reason for the increase of the cyclic fatigue life of the 2d generalized plane strain and 3d analyses in comparison to the conventional 2d plane strain analysis can be seen in Fig 7: Obviously, the conventional 2d plane strain analysis (blue line in Fig 7) shows the largest cyclic strain difference. The reason for this large plastic deformation is the plane strain condition in thickness direction of the model:

$$\varepsilon_{zz} = 0 \tag{7}$$

As a result of this vanishing axial strain, the deviatoric part of the stress tensor, which controls the plastic deformation, is comparatively large.

In reality, due to the low temperature of the nickel jacket during the hot run of approximately $70\,K$, the engine certainly shows a contraction of the combustion chamber not only in radial and circumferential direction, but in axial direction as well. As the material behavior is isotropic, this contraction in axial direction will be similar to the contraction in radial and circumferential direction of the combustion chamber. Due to this isotropic deformation or the wall material, the really occuring hydrostatic part of the stress tensor is larger than the hydrostatic stress part, obtained by assuming the conventional plane strain condition according to equation (7). This increase of the hydrostatic stress part has to be compensated by a decrease of the deviatoric stress part. This reduced deviatoric part of the stress tensor leads to a decrease of the cyclic plastic deformation.

Therefore, the 2d generalized plane strain and the 3d analysis, which do not assume equation (7), certainly obtain a better coincidence with the real deformation of the combustion chamber than the conventional 2d plane strain analysis. This consideration is confirmed by the smaller cyclic strain differences of the green and red line in Fig 7 in comparison to the blue line.

Reason for increase of the quasi static fatigue

In case the 2d analyses at point E are considered, the circumferential strain ε_{end} at the end of the cycle is smaller than the strain ε_{begin} at the beginning of the cycle. This is clearly indicated by the end points of the blue and the green line in the lower diagram in Fig 7, which are situated in the negative strain range. As a result, the strain difference $\varepsilon_{end} - \varepsilon_{begin}$ becomes negative at point E and therefore, the quasi static fatigue part is set to zero by the maximum function in equation (2). For the 3d analysis, the strain difference $\varepsilon_{end} - \varepsilon_{begin}$ is positive at point E, but very small. Therefore, the quasi static failure part can be neglected at point E for the 3d analysis as well.

The stress-strain curves for point D (upper diagram in Fig 7) meet at approximately the same point at the end of the post cooling process (point with maximum strain and maximum stress value of the diagram). Therefore, the material behavior during the relaxation phase is mainly responsible for the variation of the strain difference $\varepsilon_{end} - \varepsilon_{begin}$, which determines the quasi static failure part in equation (2). Due to the moderate temperature difference between the post cooling and the rest phase of less than $300\,K$, the deformation of the combustion chamber wall is mainly elastic in this phase of the cyclic deformation. By a detailed analysis of the elastic material tensor under the assumption of an isotropic thermal straining of the wall material, it can be shown, that the slope of the stress-strain curve is larger for the conventional 2d plane strain analysis in comparison to the 2d generalized plane strain and the 3d analysis as visible in the upper right corner of the upper diagram in Fig 7. This large slope of the stress strain curve during the relaxation phase of the combustion chamber leads leaves the positive straining at point D at the end of the post cooling phase nearly unchanged for the conventional 2d plane strain analysis. Therefore, the quasi static failure part is larger for the 2d plane strain analysis in comparison to the 2d generalized plane strain and the 3 d analysis of the combustion chamber wall.

Summary

2d plane strain, 2d generalized plane strain and 3d Finite Element analyses of rocket combustion chamber walls were compared and the influence to the post processing life time estimation was shown.

Outlook

Future developments at DLR Lampoldshausen are e.g. aimed at the improvement of the accuracy of the thermal and structural analyses and life time estimation methods. A series of improvements is possible for the thermo mechanical analysis and life time estimation of the combustion chamber wall:

- application of an improved material model including a combination of a multilinear isotropic hardening and nonlinear kinematic hardening instead of the currently used material model, assuming only a multilinear elasto-plastic material behavior with isotropic hardening,
- structural Finite Element analysis of a series of cycles,
- taking into account the hydrogen embrittlement of the material,
- application of a multi-axial life time estimation method

Also, optimization procedures will be applied in order to give recommendations for a combustion chamber design, which leads to an increased life time.

References

[1] D. Kuhl, J.R. Riccius and O.J. Haidn. Thermomechanical Fluidstructure analysis and mathematical optimization techniques applied to cryogenic liquid rocket engine design. In O.J. Haidn, editor, *International Symposium on Liquid Space Propulsion, Heilbronn*, 2000.

[2] Riccius, J.R., Hilsenbeck, M.R. and Haidn, O.J., Optimization of geometric parameters of cryogenic liquid rocket combustion chambers. *37th AIAA/ASME/SAE/ASEE JPC, AIAA-01-3408*, 2001.

[3] Riccius, J.R., Jouinot, P. and Gantschenko, V. Elasto-plastic and fatigue tests of a typical combustion chamber material with different sample geometries. *4th International Conference on Launcher Technology "Space Launcher Liquid Propulsion"*, Liege Belgium, (2002).

[4] Riccius, J.R. and Haidn, O.J., Determination of linear and nonlinear parameters of combustion chamber wall materials. *39th AIAA/ASME/SAE/ASEE Joint Propulsion Conference, AIAA-03-4901*, 2003.

[5] Bartz, D.R., A simple equation for rapid estimation of rocket nozzle convective heat transfer coefficients. *Jet Propulsion*, 27:49–51, 1957.

[6] A. Woschnak, D. Suslov and M. Oschwald, Experimental and Numerical Investigations of Thermal Stratification Effects, AIAA 2003-4615, *39th AIAA/ASME/SAE/ASEE JPC*, 2003 Huntsville, AL

[7] J.R. Riccius, O.J. Haidn and E.B. Zametaev, Influence of time dependent effects on the estimated life time of liquid rocket combustion chamber walls, AIAA 2004-3670, *40th AIAA/ASME/SAE/ASEE JPC*, July 2004 Fort Lauderdale, Florida.

[8] M. Oschwald, D. Suslov and A. Woschnak, Einfluss der Temperaturabhängigkeit der Materialeigenschaften auf den Wärmehaushalt in regenerativ gekühlten Brennkammern, DGLR-2004-111, *Deutscher Luft- und Raumfahrtkongress*, Dresden, September 2004.

[9] Jouinot, P., Gantschenko, V., Inglebert, G. and Riccius, J.: Material damage induced by environment and temperature and identification process. *Forth European Congress on Computational Methods in Applied Sciences and Engineering*, ECCOMAS 2004, P. Neittaanmäki, et. al., Jyväskylä, July 2004.

[10] Rudis, M.A. and Riccius, J.R., Liquid Rocket Engine Component Failure Probability and Residual Life Prediction at Thermal and Mechanical Cyclic Loading. *Forth European Congress on Computational Methods in Applied Sciences and Engineering*, ECCOMAS 2004, P. Neittaanmäki, T. Rossi, S. Korotov, E. Oñate, J. Périaux, and D. Knörzer (eds.), Jyväskylä, July 2004.